Controlled Intracellular Self-Assembly and Disassembly of ^{19}F Nanoparticles for MR Imaging of Caspase 3/7 in Zebrafish

Yue Yuan,[†,⊥] Hongbin Sun,[‡,⊥] Shuchao Ge,[§,⊥] Mengjing Wang,[†] Hongxin Zhao,[‡] Lin Wang,[§] Linna An,[†] Jia Zhang,[†] Huafeng Zhang,[§] Bing Hu,[*,§] Junfeng Wang,[*,‡] and Gaolin Liang[*,†]

[†]CAS Key Laboratory of Soft Matter Chemistry, University of Science and Technology of China, 96 Jinzhai Road, Hefei, Anhui 230026, China, [‡]High Magnetic Field Laboratory, Hefei Institutes of Physical Science, Chinese Academy of Sciences, 350 Shushanhu Road, Hefei, Anhui 230031, China, and [§]School of Life Sciences, University of Science and Technology of China, Hefei, Anhui 230027, China. [⊥]These authors contributed equally.

ABSTRACT

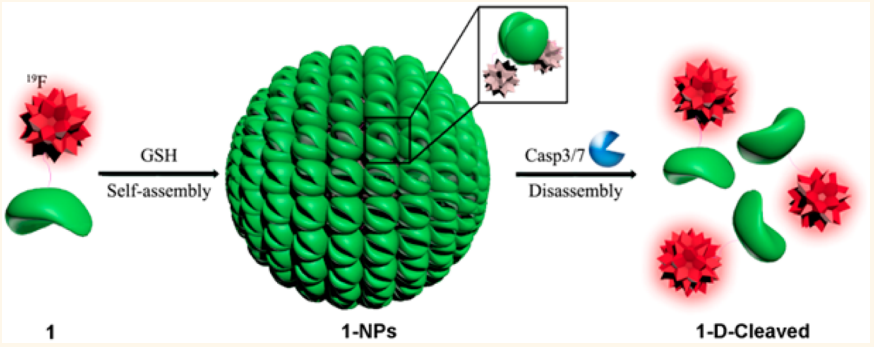

Compared to ^{1}H MRI, ^{19}F MRI provides higher selectivity but lower sensitivity. Therefore, the need to inject high doses of the ^{19}F probe to improve its sensitivity for *in vivo* diagnosis remains a challenge. A "smart" strategy is needed that could locally concentrate a low-dose ^{19}F probe while avoiding the fast transverse relaxation of the probes. Locally self-assembling and disassembling ^{19}F nanoparticles may be an optimal measure to achieve this goal. Herein, we report a dual-functional probe 1 for glutathione (GSH)-controlled self-assembly and subsequent caspase 3/7 (Casp3/7)-controlled disassembly of formed nanoparticles (*i.e.*, 1-NPs). Consecutive assembly and disassembly of 1-NPs translate to "off" and "on" ^{19}F magnetic resonance (MR) signal states, respectively. Employing this smart strategy, we successfully used 1 for the consecutive detection of GSH and Casp3/7 activity *in vitro* and in cells and imaging Casp3/7 activity in cells and in zebrafish at low doses with a 14.1 T magnetic field.

KEYWORDS: ^{19}F MRI · self-assembly · disassembly · Casp3/7 · zebrafish

Magnetic resonance imaging (MRI) is one of the most frequently used imaging techniques due to its noninvasive nature, intrinsic soft tissue contrast, superior imaging resolution, and avoidance of ionizing radiation.[1−5] Conventional clinical MRI detects ^{1}H nuclei, a majority of which reside in water and fat within the human body, and many unique nanoprobes have been recently developed for this purpose.[6−8] Other active nuclei, such as ^{13}C, ^{19}F, ^{23}Na, ^{72}As, and ^{129}Xe, can also be used in MRI detection.[9,10] ^{19}F magnetic resonance imaging (^{19}F MRI) is receiving great attention because it has NMR sensitivity similar to that of ^{1}H (83% relative to ^{1}H) and offers the highest sensitivity next to ^{1}H.[11,12] Moreover, the endogenous ^{19}F concentration in tissues is generally below the detection limit of ^{19}F MRI (usually less than 10^{-3} μmol/g wet tissue weight). This lack of background signal in body tissues gives ^{19}F MRI a high contrast-to-noise ratio and specificity for the detection of exogenous ^{19}F contrast agents. These features provide ^{19}F with promising potential in various clinical applications, such as cell tracking for stem-cell-based

* Address correspondence to bhu@ustc.edu.cn, junfeng@hmfl.ac.cn, gliang@ustc.edu.cn.

Received for review November 3, 2014 and accepted December 28, 2014.

Published online December 29, 2014
10.1021/nn5062657

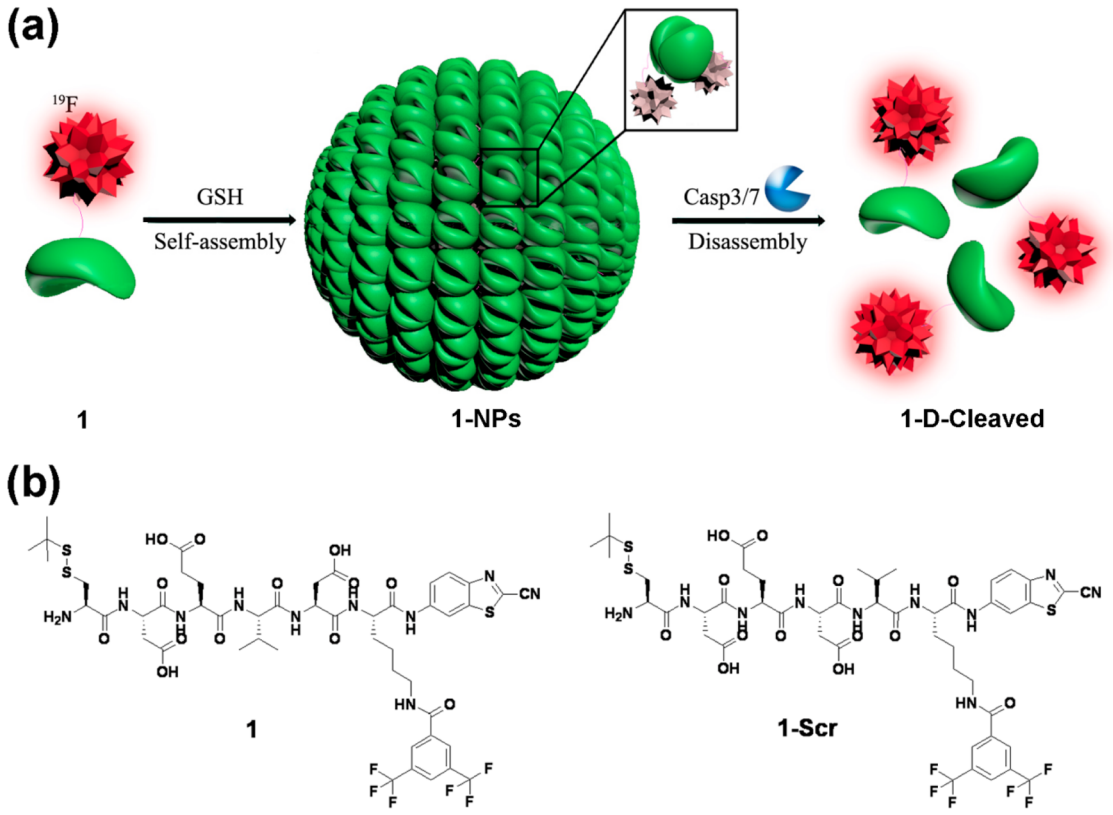

Figure 1. (a) Schematic illustration of GSH-controlled self-assembly to turn ^{19}F NMR signals "off" and Casp3/7-controlled disassembly of ^{19}F NPs to turn ^{19}F NMR signals "on". (b) Chemical structures of 1 and 1-Scr.

therapies and lung and kidney imaging using perfluorocarbons.[13−15]

To date, a variety of fluorinated compounds have been developed for ^{19}F NMR/MRI to assess biomarkers and biological events, such as gene transfection,[16] protein expression monitoring,[17,18] enzymatic activity,[19,20] pH measurement,[21] and oxidative environment alteration.[22] However, a high dose of the ^{19}F MRI probe is generally required to generate enough signal in the region of interest. This current shortcoming calls for "smart" strategies that can achieve a high local concentration of ^{19}F at the target sites with a low injection dose.

Recently, Hamachi and co-workers reported the use of supramolecular ^{19}F-containing nanoparticles for protein detection with a sharply activated ^{19}F NMR/MRI signal: the target protein binding to the ^{19}F nanoparticles leads to the disassembly of the nanoparticles, turning the ^{19}F NMR/MRI signal on.[17] Kikuchi and co-workers designed a paramagnetic relaxation-based ^{19}F MRI probe whose fluorine signal was activated upon caspase 3 (Casp3) cleavage of its DEVD sequence.[19] In our previous study, we also designed a fluorescence probe which is subjected to glutathione (GSH)-controlled self-assembly and Casp3 disassembly of nanoparticles.[23] However, due to the fluorescence resonance energy transfer within a single particle, self-assembly and subsequent disassembly of the nanoparticles resulted in "on−on" fluorescence signals instead of "off−on" signals as expected. Inspired by these works mentioned above, we herein report an enzyme-activatable ^{19}F NMR/MRI probe (Cys(StBu)-Asp-Glu-Val-Asp-Lys(FMBA)-CBT (**1**); Figure 1), whose ^{19}F NMR/MRI signal can be switched off by reduction-controlled self-assembly and switched on by the protease-controlled disassembly of their fluorinated nanoparticles (**1-NPs**) to sequentially detect GSH and caspase 3/7 (Casp3/7) activity. The advantage of this smart probe is that highly concentrated ^{19}F signals can be easily obtained at the target site after its nanoparticles are disassembled.

We used intracellular Casp3/7 to disassemble the **1-NPs**, intensely activating the ^{19}F signal to the "on" state to detect Casp3/7 activity with high sensitivity. A biocompatible, highly efficient condensation was employed to initiate the intracellular self-assembly of **1-NPs**, and biocompatible starting materials were used to synthesize the probes, making the whole system biocompatible.[24,25] The reason that we designed **1** for the consecutive detection of GSH and Casp3/7 is that high endogenous GSH can be applied to assemble ^{19}F nanoparticles to locally produce high ^{19}F concentration in the stealth state, and activation of Casp3/7 turns the signal "on". Employing this "smart" strategy of self-assembly and disassembly, we successfully imaged Casp3/7 in zebrafish models of apoptosis at low doses, under 14.1 T with the multifunctional probes **1**.

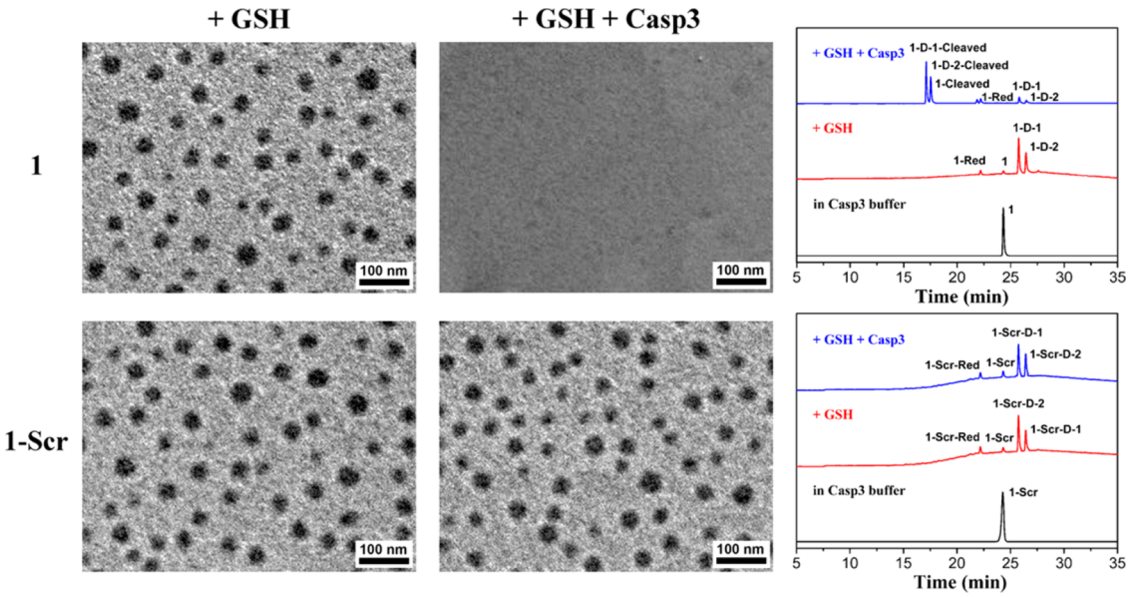

Figure 2. Left column: TEM images of 1-NPs (top) and 1-Scr-NPs (bottom) (100 μL of 500 μM 1 or 1-Scr treated with 2 mM GSH for 30 min). Middle column: TEM images of 1-NPs (top) and 1-Scr-NPs (bottom) after being incubated with 10 nmol/U Casp3 at 37 °C for 6 h. Right column: HPLC traces of 100 μL of 500 μM 1 (top) or 1-Scr (bottom) in Casp3 buffer (black), 100 μL of 500 μM 1 or 1-Scr treated with 2 mM GSH for 30 min (red), and 100 μL of 500 μM 1 or 1-Scr first treated with 2 mM GSH for 30 min and then incubated with 10 nmol/U Casp3 at 37 °C for 6 h (blue).

RESULTS AND DISCUSSION

Rationale of the Design. On the basis of a biocompatible condensation reaction recently developed by Rao and co-workers,[24,26] we designed our ^{19}F probes with the following components, as shown in Figure 1: a disulfide cysteine (Cys) motif, a 2-cyanobenzothiazole (CBT) motif, a DEVD substrate for Casp3/7 cleavage, and an FMBA motif conjugated to the side chain of lysine (Lys) to generate the ^{19}F NMR signal. Due to the advantage of an abundance of GSH in cells, the probes will first be reduced to expose the reactive 1,2-aminothiol groups after entering the cell. Then, the condensation reaction between the free 1,2-aminothiol group and the cyano group of the CBT motif will occur as demonstrated previously,[24,25] and the condensed products will self-assemble into ^{19}F nanoparticles (**1-NPs**). Thus, the local concentration of ^{19}F inside cells will increase. Correspondingly, the ^{19}F signal of the probes will be switched "off" upon the formation of the nanoparticles due to the fast transverse relaxation of the ^{19}F magnetic spins. In apoptotic cells, there is a high level of Casp3/7 activity. The highly expressed Casp3/7 enzymes will cleave their DEVD substrates within the **1-NPs** and disassemble the nanoparticles, switching on the ^{19}F NMR signals. A detailed schematic illustration accompanied by the chemical structures to show the rationale of the design is shown in Figure S1 (Supporting Information). We also synthesized a scrambled control, Cys(StBu)-Asp-Glu-Asp-Val-Lys(FMBA)-CBT (**1-Scr**), an inactive isomer of **1** to be studied in parallel. The synthetic routes and characterization of **1** and **1-Scr** are described in the Supporting Information (Figures S2−S5).

GSH-Controlled Self-Assembly and Casp3-Controlled Disassembly of 1-NPs. After the syntheses and characterization of **1** and **1-Scr**, we validated the GSH-controlled condensation and self-assembly of the ^{19}F nanoparticles (NPs). **1** or **1-Scr** was dissolved in 200 μL of Casp3 buffer (pH 7.4) to a final concentration of 500 μM and equally divided into two parts, one for GSH-controlled self-assembly of NPs and the other for Casp3 treatment after the NP formation. After the addition of 2 mM GSH for 30 min at 37 °C, the disulfide bond of **1** or **1-Scr** was reduced by GSH, initiating the condensation reaction and subsequent self-assembly of **1-NPs** or **1-Scr-NPs**. The formation of **1-NPs** or **1-Scr-NPs** was clearly observed with a transmission electron microscope (TEM). The TEM images showed that the fluorine NPs of **1** (*i.e.*, **1-NPs**) and **1-Scr** (*i.e.*, **1-Scr-NPs**) have average diameters of 27 ± 6 and 26 ± 6 nm, respectively (left column of Figure 2). Concentration of GSH seemed to affect the size of the NPs obtained. At GSH concentrations of 1 and 4 mM, **1-NPs** have mean diameters of 21 ± 7 and 31 ± 9 nm respectively, suggesting that the size of the nanoparticles increased with the increase of the concentration of GSH (Figure S6). However, the size of **1-NPs** seemed to not be affected by time (Figure S7), suggesting that the process of self-assembly of the NPs could be accomplished within a short time. We then incubated the 100 μL of NP dispersions with 10 nmol/U Casp3 at 37 °C for 6 h. From TEM images, we clearly observed that **1-NPs** were digested by Casp3 and disassembled, whereas the **1-Scr-NPs** remained unchanged (middle column of Figure 2), suggesting that **1-NPs** are susceptible to Casp3 but that **1-Scr-NPs** are impervious. To further confirm that the disassembly of

1-NPs was induced by Casp3 cleavage, we pretreated Casp3 with a caspase inhibitor (CI, Z-VAD-FMK) at 20 μM for 10 min and then incubated Casp3 with the NPs. Clearly, we found that **1-NPs** were unactivated, and the HPLC trace only showed the condensation products of **1** by GSH (*i.e.*, **1-D-1** and **1-D-2**) but no Casp3-cleaved products (Figure S8). The self-assembly and disassembly of **1-NPs** or **1-Scr-NPs** were also confirmed with UV−vis spectroscopy and dynamic light scattering (Figures S9−S11). To chemically validate the GSH-controlled condensation and subsequent Casp3 cleavage, we directly injected the above incubation mixtures into a high-performance liquid chromatography (HPLC) system and collected the peaks for matrix-assisted laser desorption/ionization mass spectroscopic analysis. After 100 μL of 500 μM **1** was treated with 2 mM GSH, we identified the peaks on the HPLC trace at retention times of 25.8 and 26.4 min as the two isomeric condensation products of **1** (*i.e.*, **1-D-1** and **1-D-2**, top right panel of Figure 2 and Figure S12). The tiny peak at 22.2 min was identified as the reduction product of **1** by GSH before condensation (*i.e.*, **1-Red**, Figure S13). After the addition and incubation of 10 nmol/U Casp3 with the mixture at 37 °C for 6 h, we identified two new peaks at retention times of 17.1 and 17.5 min as the corresponding products of Casp3 cleavage of **1-D-1** and **1-D-2** (*i.e.*, **1-D-1-Cleaved** and **1-D-2-Cleaved**, top right panel of Figure 2 and Figure S14). For comparison, as shown in the bottom right panel of Figure 2, 100 μL of 500 μM **1-Scr** treated with 2 mM GSH also resulted in two isomeric condensation products of **1-Scr** with retention times of 25.8 and 26.4 min on the HPLC traces (*i.e.*, **1-Scr-D-1** and **1-Scr-D-2**, Figure S15). Similarly, the small peak at 22.2 min was identified as the reduction product of **1-Scr** by GSH before condensation (*i.e.*, **1-Scr-Red**, Figure S16). Importantly, further addition and incubation of Casp3 with the condensation mixture of **1-Scr** did not induce any change in its HPLC traces, suggesting that the condensation products of **1-Scr** (*i.e.*, **1-Scr-D-1** and **1-Scr-D-2**) were not cleavable by Casp3 (bottom right panel of Figure 2). We also tested the susceptibility of **1** and **1-Scr** to Casp3, and the results showed that **1**, but not **1-Scr**, was cleavable by Casp3 (Figures S17−S19).

^{19}F NMR Spectra of 1 for the Detection of GSH and Casp3/7 *in Vitro* and in Cells. The ^{19}F NMR spectra of **1**, **1** treated with GSH (*i.e.*, the formation of **1-NPs**), and **1** treated with GSH followed by Casp3 (*i.e.*, hydrolysis and disassembly of **1-NPs**) are shown in Figure 3a. We observed the disappearance of the ^{19}F NMR signal of **1** at −61.8 ppm after being treated with GSH, suggesting that the formation of **1-NPs** induces fast transverse relaxation of ^{19}F magnetic spin due to slower molecular tumbling. After the incubation of **1-NPs** with Casp3, the ^{19}F NMR signal of **1** at −61.8 ppm recovered. To further confirm that the recovered ^{19}F NMR signal was due to the hydrolysis and disassembly of **1-NPs** by

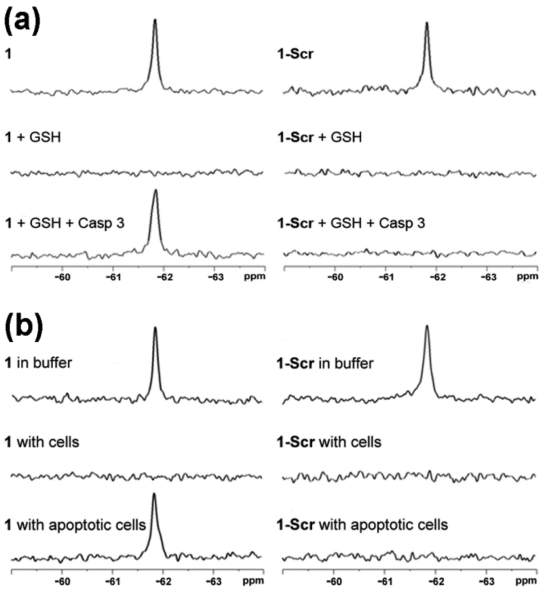

Figure 3. (a) ^{19}F NMR spectra of 1 or 1-Scr at 500 μM in 100 μL of Casp3 buffer (top), in the presence of 2 mM GSH for 30 min (middle), and in the presence of 2 mM GSH for 30 min followed by incubation with 50 nmol/6U Casp3 at 37 °C for 6 h (bottom). (b) ^{19}F NMR spectra of 1 or 1-Scr at 500 μM in 100 μL of RIPA lysis buffer (top), in 100 μL of cell lysate after being incubated with HepG2 cells at 37 °C for 30 min (middle), and in 100 μL of cell lysate after being incubated with apoptotic HepG2 cells at 37 °C for 30 min (bottom). The ^{19}F molarity used here was 3 mM.

Casp3, we pretreated Casp3 with CI at 20 μM for 10 min and then incubated Casp3 with the NPs. We found that the "off" signal of **1-NPs** remained off (Figure S21). In comparison, as shown in Figure 3a, the treatment of **1-Scr** with GSH also induced the disappearance of the ^{19}F NMR signal at −61.8 ppm, implying that **1-Scr-NPs** were formed. However, the ^{19}F NMR signal could not be recovered after further incubation of **1-Scr-NPs** with Casp3 under the same conditions. When we separately incubated **1** or **1-Scr** in the presence of a mixture of 2 mM GSH and 50 nmol/6U Casp3 and studied their ^{19}F NMR spectra over time, we found that the ^{19}F NMR signal of **1** at −61.8 ppm first disappeared at 10 min and then started to recover at 1 h (Figure S22a). In contrast, the ^{19}F NMR signal of **1-Scr** at −61.8 ppm remained "off" during the 5 h observation (Figure S22b). TEM images of **1** in the presence of the mixture of 2 mM GSH and 50 nmol/6U Casp3 showed the appearance of **1-NPs** at 10 min and the disappearance of the NPs at 5 h (Figure S23). These results suggested that the GSH-controlled assembly and subsequent Casp3-controlled disassembly of **1-NPs** successively turn the ^{19}F NMR signals of **1** "off" and "on", respectively, making **1** applicable for the consecutive detection of GSH and Casp3 *in vitro*. The process of the ^{19}F NMR signal of **1** changing from state "off" to "on" could be monitored stepwise by changing the concentrations of GSH and Casp3 added (Figure S24). The temporal dynamics of Casp3-

mediated induction of the "on" state was also tracked and shown in Figure S25. After *in vitro* cell-free studies, we then used **1** to detect GSH and Casp3/7 in HepG2 cells. For these studies, 4×10^6 live HepG2 cells were trypsinized and collected into a 5 mL centrifuge tube and then incubated with 500 μM of **1** or **1-Scr** in serum-free culture medium at 37 °C for 30 min. The cells were then lysed with radio-immunoprecipitation assay (RIPA) lysis buffer, and the supernatants were collected for ^{19}F NMR spectrometric analysis. As shown in Figure 3b, compared with the ^{19}F NMR signals of **1** or **1-Scr** seen in RIPA buffer at −61.8 ppm, the ^{19}F NMR signals of **1** and **1-Scr** incubated with healthy HepG2 cells disappeared, indicating the GSH-controlled formation of **1-NPs** and **1-Scr-NPs**, respectively. Following a previously reported method, we exposed the healthy HepG2 cells to 254 nm UV light at 10 000 $\mu J \cdot cm^{-2}$ and waited 50 min for the full activation of Casp3/7 in the cells.[27] The cells were then treated with **1** or **1-Scr** as described above. As shown in Figure 3b, the ^{19}F NMR signal of **1** at −61.8 ppm incubated with apoptotic HepG2 cells reappeared, whereas the peak did not appear for cells treated with **1-Scr**. To rule out other factors (*e.g.*, other proteases) that could induce the signal to turn on, we pretreated the apoptotic cells with CI before incubating them with **1** or **1-Scr** and found that **1** remained in an "off" state (Figure S26). This result indicated that **1** could be applied to specifically detect Casp3/7 activity in cells. To validate that the self-assembly and disassembly of **1-NPs** in apoptotic cells could locally increase the ^{19}F NMR signal-to-noise (S/N) ratio in the cells, we also incubate compound **D** (*i.e.*, precursor of **1**, not able to self-assemble into NPs but susceptible to Casp3/7, Scheme S1) with apoptotic HepG2 cells. The results indicated that the S/N ratio of **D** was less than half of that of **1** (Figure S27). The blank HepG2 cell lysate, which did not have any detectable ^{19}F NMR signal, was used as a control (Figure S28). HPLC analyses were employed throughout the experiments to validate the GSH-controlled condensation and Casp3/7 cleavage (Figure S29). 3-(4,5-Dimethylthiazol-2-yl)-2,5-diphenyltetrazolium bromide assay indicated that, up to 1 mM and for 3 days, none of **1**, **1-Scr**, **1-NPs**, or **1-Scr-NPs** showed cytotoxicity to HepG2 cells (Figure S30), suggesting that our probes are biocompatible.

^{19}F MR Imaging of GSH and Casp3/7 in Cells Treated with 1. The on, off, and on ^{19}F NMR signals, corresponding to **1** by itself, **1** with healthy HepG2 cells, and **1** with apoptotic HepG2 cells, respectively, were also clearly imaged with ^{19}F MRI at 14.1 T. As shown in Figure 4, after the incubation of 2.5 mM of **1** or **1-Scr** with 8×10^7 HepG2 cells at 37 °C for 30 min, ^{19}F MRI signals disappeared in both cases (middle column of Figure 4). However, the incubation of **1** with apoptotic HepG2 cells restored ^{19}F MRI signals, whereas those of **1-Scr** remained "off" (right column in Figure 4). This result clearly demonstrated that **1** could be used to image Casp3/7 activity in apoptotic cells.

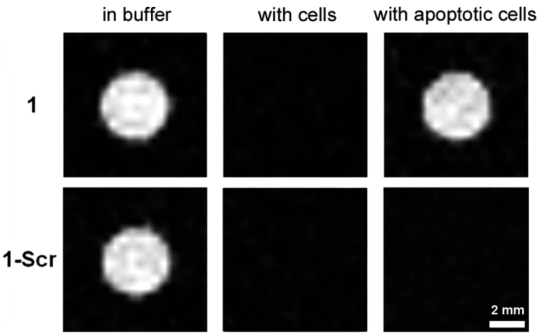

Figure 4. ^{19}F MR imaging of 1 (top) or 1-Scr (bottom) at 2.5 mM in 500 μL of RIPA lysis buffer (left), in 500 μL of cell lysate after being incubated with HepG2 cells at 37 °C for 30 min (middle), and in 500 μL of cell lysate after being incubated with apoptotic HepG2 cells at 37 °C for 30 min (right). The ^{19}F molarity used here was 15 mM.

^{19}F MR Imaging of Casp3/7 Activity in Zebrafish Treated with 1. **1** was applied to the ^{19}F MR imaging of Casp3/7 activity *in vivo* using high magnetic field strength (14.1 T). A zebrafish model was chosen for two reasons. First, the tail apoptosis model of zebrafish is well-established and easily verified; second, the size of a 4 month old zebrafish is appropriate for a 5 mm (Φ) NMR tube for micro-MRI. It was reported that Casp3/7-positive cells are activated near the lesion within a few hours of the amputation of a zebrafish tail.[28] Using acridine orange staining to monitor the apoptotic process in a tail lesion (Figures S32 and S33), 3 h post-amputation was chosen as the optimized condition for our experiment.[28−30] In a typical experiment, 3 h after tail amputation, zebrafish were anesthetized in 0.2 mg/mL tricaine solution for 5 min. Then, 10 μL of **1** or **1-Scr** (dissolved in DMSO) was injected into the enterocoelia of a zebrafish at a dose of 2.1 g/kg. Toxicity study indicated that 100% of zebrafish injected with **1** at this dosage survived for 3 days, while 100% of the zebrafish injected with **1-Scr** at this dosage survived for 1 day and 95% of them survived for 3 days (Figure S31). Two hours after the injection, water on the fish was absorbed with tissue paper before the fish was deposited into the 5 mm (in diameter) NMR tube for ^{1}H MRI in a Bruker MRI/NMR system at 14.1 T (600 MHz proton frequency). After ^{1}H MRI, the zebrafish was immersed and postfixed in 4% paraformaldehyde for ^{19}F MR imaging. We observed strong ^{19}F MRI signals located at (or near) the lesions in zebrafish (topmost row in Figure 5), whereas tail-amputated zebrafish injected with **1-Scr** did not show any ^{19}F MRI signals (top middle row of Figure 5). These data indicate that the GSH-controlled, self-assembled **1-NPs** were cleaved and disassembled by Casp3/7 in apoptotic zebrafish, turning on the ^{19}F MRI signals at the locations of Casp3/7 activity. The **1-Scr-NPs**, in contrast, were not cleavable by Casp3/7 and thus could not reveal

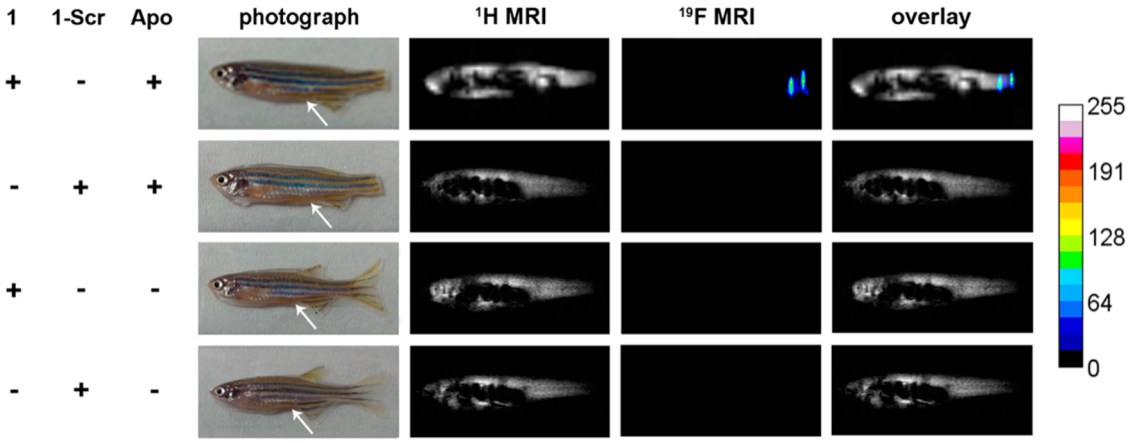

Figure 5. Topmost row: 2.1 g/kg of 1 (10 μL, dissolved in DMSO) was injected into the enterocoelia of zebrafish 3 h after tail amputation. Top middle row: 2.1 g/kg of 1-Scr (10 μL, dissolved in DMSO) was injected into the enterocoelia of zebrafish 3 h after tail amputation. Bottom middle row: 2.1 g/kg of 1 (10 μL, dissolved in DMSO) was injected into the enterocoelia of a healthy zebrafish. Bottom-most row: 2.1 g/kg of 1-Scr (10 μL, dissolved in DMSO) was injected into the enterocoelia of a healthy zebrafish. White arrows indicate the injection sites. The ^{19}F molarity used here was about 10.5 mM.

Casp3/7 activity. Another control compound **D**, which cannot self-assemble into NPs but is susceptible to Casp3, only showed indiscriminative ^{19}F MRI signals in apoptotic zebrafish with much lower S/N ratio than that of **1** (Figure S34). To further validate that the ^{19}F MRI signals were due to the activation of Casp3/7 at the lesions, **1** or **1-Scr** was also injected into a healthy zebrafish at the same dose. No ^{19}F MRI signals could be observed from any part of the zebrafish (bottom middle and bottom-most rows of Figure 5). Using ^{19}F NMR spectra of the organs of healthy zebrafish injected with **1** to study the metabolism of **1-NPs** in zebrafish, we found that the NPs were mostly concentrated in the spleens of the zebrafish until 24 h (Figure S35). To factor out other influences (*e.g.*, other proteases) that could turn the ^{19}F MRI signal "on", we pretreated the apoptotic zebrafish with CI before the injection of **1** and found that the ^{19}F MRI signals of **1** were totally turned "off" (Figure S36). This result indicated that the "on" signals were induced by Casp3/7. Furthermore, to overcome the ^{19}F MRI signal depletion induced by the GSH-controlled self-assembly of **1-NPs**, we found that a nearly 7-fold higher dosage of **1** (14.1 g/kg) was necessary to obtain ^{19}F MRI signals from a healthy zebrafish (Figure S37).

CONCLUSIONS

In summary, by the rational design of a biocompatible dual-functional fluorine probe **1**, we have developed a "smart" method of GSH-controlled assembly and Casp3/7-controlled disassembly of **1-NPs** that turns the ^{19}F NMR signal "off" and then "on" for the sequential detection of GSH and Casp3/7 *in vitro* and in cells. With the ^{19}F NMR data obtained, we also successfully used **1** for the ^{19}F MRI detection of Casp3/7 activity in zebrafish at low doses under 14.1 T. These *in vitro* and *in vivo* studies suggest that this multifunctional probe might be applied to ^{19}F MRI of chemotherapeutic efficiency of tumors in routine preclinical studies or even in patients.

EXPERIMENTAL SECTION

^{19}F Nuclear Magnetic Resonance Methods. ^{19}F NMR experiments were performed on a Bruker Ascend WB 600 MHz spectrometer using a 4 mm broad-band N−C/F/H MAS probe. All ^{19}F NMR spectra were acquired with 3 s delays, accumulating 256 scans for a one-dimensional (1D) ^{19}F spectrum. The 1D ^{19}F spectrum was acquired with one pulse program with a 90 pulse width of 5.5 μs. ^{19}F chemical shifts were referenced to trifluoroacetic acid (−76.5 ppm). All data were acquired and analyzed with Bruker's Topspin 3.1 software. All experiments were performed at 25 °C.

^{1}H Magnetic Resonance Imaging Methods. ^{1}H magnetic resonance images of zebrafish in the topmost row of Figure 5 were obtained by flash method with repetition time/echo time of 120/1.53 ms, field of view of 6 × 6 cm without slice selection and accumulation, and a matrix size of 128 × 48. The excitation pulse width was 2740 Hz. ^{1}H magnetic resonance images of zebrafish in the bottom rows of Figure 5 were obtained by a flash method with repetition time/echo time of 120/1.60 ms, field of view of 2.2 × 0.5 cm without slice selection and accumulation, and a matrix size of 128 × 128. The excitation pulse width was 2740 Hz. The images were obtained at 25 °C.

^{19}F Magnetic Resonance Imaging. Images were acquired on a Bruker Ascend WB 600 MHz spectrometer using a Bruker Micro 5 imaging probe with triple axis gradients (maximum strength 200 G/cm) and an 8 mm diameter RF saddle coil. ^{19}F magnetic resonance images of phantom samples in Figure 4 were obtained by fast spin−echo with repetition time/echo time of 2000/7.9 ms using flash imaging pulse sequence; flip angle was 180°; field of view was 3 × 3 cm; slice thickness was 5 mm; matrix size was 64 × 64, and the number of accumulations was 256 (9 h, 6 min, 8 s). The excitation pulse width was 2740 Hz. All images were acquired and analyzed using Bruker's Para Vision 5.1 software. The original images were cropped and combined to create Figure 4.

^{19}F magnetic resonance images of zebrafish in Figure 5 were acquired by a flash method with repetition time/echo time of 100/3.56 ms; the flip angle was 30°; the field of view was 6 × 6 cm; slice thickness was 5 mm; matrix size was 128 × 48,

and the number of accumulations was 49 500 (66 h, 0 min, 0 s). The excitation pulse width was 12 500 Hz. All experiments were conducted at 25 °C.

^{19}F NMR Test *in Vitro*. **1** or **1-Scr** was dissolved in 100 μL of Casp3 buffer (pH 7.4) to a final concentration of 500 μM, then the ^{19}F NMR spectra were monitored after the addition of 2 mM GSH for 30 min at 37 °C. After the incubation of the above-obtained 100 μL of **1-NPs** or **1-Scr-NPs** dispersions with 50 nmol/6U Casp3 at 37 °C for 6 h, the mixtures were transferred to NMR tubes for ^{19}F NMR spectroscopic measurements.

Cell Experiment for ^{19}F NMR. For healthy HepG2 cells, 4×10^6 live HepG2 cells were trypsinized and collected into a 5 mL centrifuge tube. After incubation of 500 μM **1** or **1-Scr** with HepG2 cells in serum-free culture medium at 37 °C for 30 min, the cells were centrifuged (1000 rpm, 5 min) and washed three times with PBS to remove the remaining probe. Then the cells were lysed with 100 μL of RIPA lysis buffer for 15 min, and the supernatants were collected for ^{19}F NMR spectrometric analysis. For apoptotic HepG2 cells, the healthy HepG2 cells were exposed to 254 nm UV light at 10 000 $\mu J \cdot cm^{-2}$ and waited 50 min for the full activation of Casp3/7 in the cells. Then the cells were treated with **1** or **1-Scr**, and the cell lysates were collected as described above. For CI-treated apoptotic HepG2 cells, the healthy HepG2 cells were preincubated with 100 μM CI for 10 min, and the cells were then exposed to 254 nm UV light at 10 000 $\mu J \cdot cm^{-2}$ and waited 50 min for the full activation of Casp3/7 in the cells. The cells were then treated with **1** or **1-Scr**, and the cell lysates were collected as described above.

Cell Experiment for ^{19}F MRI. For healthy HepG2 cells, 8×10^7 live HepG2 cells were trypsinized and collected into a 5 mL centrifuge tube. After the incubation of 2.5 mM **1** or **1-Scr** with HepG2 cells in serum-free culture medium at 37 °C for 30 min, the cells were centrifuged (1000 rpm, 5 min) and washed three times with PBS to remove the remaining probe. Then the cells were lysed with 500 μL of RIPA lysis buffer for 15 min, and the supernatants were collected for ^{19}F MRI spectrometric analysis. For apoptotic HepG2 cells, the healthy HepG2 cells were exposed to 254 nm UV light at 10 000 $\mu J \cdot cm^{-2}$ and waited 50 min for the full activation of Casp3/7 in the cells. Then the cells were treated with **1** or **1-Scr**, and the cell lysates were collected as described above.

Conflict of Interest: The authors declare no competing financial interest.

Acknowledgment. We would like to thank Dr. Long Miao for thoughtful discussions. This work was supported by Collaborative Innovation Center of Suzhou Nano Science and Technology, the National Natural Science Foundation of China (Grants 21375121, 91127036, U1332142, 21103199, and U1332136), the Fundamental Research Funds for Central Universities (WK2060190018), and the Chinese Academy of Sciences (Hundred Talents Program).

Supporting Information Available: Experimental methods and details, characterization details, HPLC conditions, Schemes S1 and S2, Figures S1−S37, and Tables S1−S5. This material is available free of charge *via* the Internet at http://pubs.acs.org.

REFERENCES AND NOTES

1. Danielson, M. A.; Falke, J. J. Use of ^{19}F NMR To Probe Protein Structure and Conformational Changes. *Annu. Rev. Biophys. Biomol. Struct.* **1996**, *25*, 163–195.
2. Thorek, D. L. J.; Ulmert, D.; Diop, N. F. M.; Lupu, M. E.; Doran, M. G.; Huang, R. M.; Abou, D. S.; Larson, S. M.; Grimm, J. Non-invasive Mapping of Deep-Tissue Lymph Nodes in Live Animals Using a Multimodal PET/MRI Nanoparticle. *Nat. Commun.* **2014**, *5*, 3097.
3. Shapiro, M. G.; Westmeyer, G. G.; Romero, P. A.; Szablowski, J. O.; Kuster, B.; Shah, A.; Otey, C. R.; Langer, R.; Arnold, F. H.; Jasanoff, A. Directed Evolution of a Magnetic Resonance Imaging Contrast Agent for Noninvasive Imaging of Dopamine. *Nat. Biotechnol.* **2010**, *28*, 264–270.
4. Bull, S. R.; Guler, M. O.; Bras, R. E.; Meade, T. J.; Stupp, S. I. Self-Assembled Peptide Amphiphile Nanofibers Conjugated to MRI Contrast Agents. *Nano Lett.* **2005**, *5*, 1–4.
5. MacDonald, T. D.; Liu, T. W.; Zheng, G. An MRI-Sensitive, Non-photobleachable Porphysome Photothermal Agent. *Angew. Chem., Int. Ed.* **2014**, *53*, 6956–6959.
6. Cheng, K.; Yang, M.; Zhang, R.; Qin, C.; Su, X.; Cheng, Z. Hybrid Nanotrimers for Dual T_1 and T_2-Weighted Magnetic Resonance Imaging. *ACS Nano* **2014**, *8*, 9884–9896.
7. Zhou, Z.; Wang, L.; Chi, X.; Bao, J.; Yang, L.; Zhao, W.; Chen, Z.; Wang, X.; Chen, X.; Gao, J. Engineered Iron-Oxide-Based Nanoparticles as Enhanced T_1 Contrast Agents for Efficient Tumor Imaging. *ACS Nano* **2013**, *7*, 3287–3296.
8. Ye, D.; Pandit, P.; Kempen, P.; Lin, J.; Xiong, L.; Sinclair, R.; Rutt, B.; Rao, J. Redox-Triggered Self-Assembly of Gadolinium-Based MRI Probes for Sensing Reducing Environment. *Bioconjugate Chem.* **2014**, *25*, 1526–1536.
9. Chakravarty, R.; Valdovinos, H. F.; Chen, F.; Lewis, C. M.; Ellison, P. A.; Luo, H.; Meyerand, M. E.; Nickles, R. J.; Cai, W. Intrinsically Germanium-69-Labeled Iron Oxide Nanoparticles: Synthesis and *In-Vivo* Dual-Modality PET/MR Imaging. *Adv. Mater.* **2014**, *26*, 5119–5123.
10. Klippel, S.; Freund, C.; Schröder, L. Multichannel MRI Labeling of Mammalian Cells by Switchable Nanocarriers for Hyperpolarized Xenon. *Nano Lett.* **2014**, *14*, 5721–5726.
11. Tirotta, I.; Dichiarante, V.; Pigliacelli, C.; Cavallo, G.; Terraneo, G.; Bombelli, F. B.; Metrangolo, P.; Resnati, G. ^{19}F Magnetic Resonance Imaging (MRI): From Design of Materials to Clinical Applications. *Chem. Rev.* **2014**, 10.1021/cr500286d.
12. Wolters, M.; Mohades, S. G.; Hackeng, T. M.; Post, M. J.; Kooi, M. E.; Backes, W. H. Clinical Perspectives of Hybrid Proton-Fluorine Magnetic Resonance Imaging and Spectroscopy. *Invest. Radiol.* **2013**, *48*, 341–350.
13. Srinivas, M.; Heerschap, A.; Ahrens, E. T.; Figdor, C. G.; de Vries, I. J. M. Imaging of Cellular Therapies. *Trends Biotechnol.* **2010**, *28*, 363–370.
14. Ruiz-Cabello, J.; Barnett, B. P.; Bottomley, P. A.; Bulte, J. W. M. Fluorine (^{19}F) MRS and MRI in Biomedicine. *NMR Biomed.* **2011**, *24*, 114–129.
15. Hu, L. Z.; Chen, J. J.; Yang, X. X.; Senpan, A.; Allen, J. S.; Yanaba, N.; Caruthers, S. D.; Lanza, G. M.; Hammerman, M. R.; Wickline, S. A. Assessing Intrarenal Non-perfusion and Vascular Leakage in Acute Kidney Injury with ^{19}F MRI and Perfluorocarbon Nanoparticles. *Magn. Reson. Med.* **2014**, *71*, 2186–2196.
16. Cui, W.; Otten, P.; Li, Y.; Koeneman, K. S.; Yu, J.; Mason, R. P. Novel NMR Approach to Assessing Gene Transfection: 4-Fluoro-2-nitrophenyl-β-D-galactopyranoside as a Prototype Reporter Molecule for β-Galactosidase. *Magn. Reson. Med.* **2004**, *51*, 616–620.
17. Takaoka, Y.; Sakamoto, T.; Tsukiji, S.; Narazaki, M.; Matsuda, T.; Tochio, H.; Shirakawa, M.; Hamachi, I. Self-Assembling Nanoprobes That Display Off/On ^{19}F Nuclear Magnetic Resonance Signals for Protein Detection and Imaging. *Nat. Chem.* **2009**, *1*, 557–561.
18. Higuchi, M.; Iwata, N.; Matsuba, Y.; Sato, K.; Sasamoto, K.; Saido, T. C. ^{19}F and ^{1}H MRI Detection of Amyloid Beta Plaques *in Vivo*. *Nat. Neurosci.* **2005**, *8*, 527–533.
19. Mizukami, S.; Takikawa, R.; Sugihara, F.; Hori, Y.; Tochio, H.; Wälchli, M.; Shirakawa, M.; Kikuchi, K. Paramagnetic Relaxation-Based ^{19}F MRI Probe To Detect Protease Activity. *J. Am. Chem. Soc.* **2008**, *130*, 794–795.
20. Keliris, A.; Mamedov, I.; Hagberg, G. E.; Logothetis, N. K.; Scheffler, K.; Engelmann, J. A Smart ^{19}F and ^{1}H MRI Probe with Self-Immolative Linker as a Versatile Tool for Detection of Enzymes. *Contrast Media Mol. Imaging* **2012**, *7*, 478–483.
21. Huang, X.; Huang, G.; Zhang, S.; Sagiyama, K.; Togao, O.; Ma, X.; Wang, Y.; Li, Y.; Soesbe, T. C.; Sumer, B. D.; et al. Multi-chromatic pH-Activatable ^{19}F-MRI Nanoprobes with Binary ON/OFF pH Transitions and Chemical-Shift Barcodes. *Angew. Chem., Int. Ed.* **2013**, *52*, 8074–8078.
22. Tanabe, K.; Harada, H.; Narazaki, M.; Tanaka, K.; Inafuku, K.; Komatsu, H.; Ito, T.; Yamada, H.; Chujo, Y.; Matsuda, T.; et al. Monitoring of Biological One-Electron Reduction by ^{19}F NMR Using Hypoxia Selective Activation of an ^{19}F-Labeled

Indolequinone Derivative. *J. Am. Chem. Soc.* **2009**, *131*, 15982–15983.
23. Huang, R.; Wang, X.; Wang, D.; Liu, F.; Mei, B.; Tang, A.; Jiang, J.; Liang, G. Multifunctional Fluorescent Probe for Sequential Detections of Glutathione and Caspase-3 *in Vitro* and in Cells. *Anal. Chem.* **2013**, *85*, 6203–6207.
24. Liang, G.; Ren, H.; Rao, J. A Biocompatible Condensation Reaction for Controlled Assembly of Nanostructures in Living Cells. *Nat. Chem.* **2010**, *2*, 54–60.
25. Ren, H.; Xiao, F.; Zhan, K.; Kim, Y.; Xie, H.; Xia, Z.; Rao, J. A Biocompatible Condensation Reaction for the Labeling of Terminal Cysteine Residues on Proteins. *Angew. Chem., Int. Ed.* **2009**, *48*, 9658–9662.
26. Ye, D. J.; Shuhendler, A. J.; Cui, L. N.; Tong, L.; Tee, S. S.; Tikhomirov, G.; Felsher, D. W.; Rao, J. H. Bioorthogonal Cyclization-Mediated *In Situ* Self-Assembly of Small-Molecule Probes for Imaging Caspase Activity *in Vivo*. *Nat. Chem.* **2014**, *6*, 519–526.
27. Billecke, C. A.; Ljungman, M. E.; McKay, B. C.; Rehemtulla, A.; Taneja, N.; Ethier, S. P. Lack of Functional pRb Results in Attenuated Recovery of mRNA Synthesis and Increased Apoptosis Following UV Radiation in Human Breast Cancer Cells. *Oncogene* **2002**, *21*, 4481–4489.
28. Gauron, C.; Rampon, C.; Bouzaffour, M.; Ipendey, E.; Teillon, J.; Volovitch, M.; Vriz, S. Sustained Production of ROS Triggers Compensatory Proliferation and Is Required for Regeneration To Proceed. *Sci. Rep.* **2013**, *3*, 2084.
29. Denning, D. P.; Hatch, V.; Horvitz, H. R. Programmed Elimination of Cells by Caspase-Independent Cell Extrusion in *C. elegans*. *Nature* **2012**, *488*, 226–227.
30. Abrams, J. M.; White, K.; Fessler, L. I.; Steller, H. Programmed Cell Death during Drosophila Embryogenesis. *Development* **1993**, *117*, 29–43.